Ultrasound Texture Analysis For Masseteric Muscle Health Evaluation

Rafael Bartolomé Méndez

March 28, 2002

Acknowledgements

Para empezar, quisiera agradecer a todos mis amigos de España que no estan relacionados con mi futura profesión que me sigan aguantando. También quisiera agardecer a aquellos telequitos que han conseguido que la carrera no fuese tan aburrida. Especial mención a las jornadas casi esotéricas en las aulas de estudio. Sólo aquellos que estábamos allí sabemos hasta donde somos capaces de llegar. Mención especial también para la gente de Lausanne. Lausanne puede llegar a ser aburrido, pero con esa gente no lo ha sido tanto y más de una vez nos hemos reido un rato largo. Por otro lado, no me puedo olvidar de las partidas de mus, de Santa Coupole (la de la una victoriosa) y de Santo Sattelite (el de los milagros).

I would like to thank all the people at the LTS and specially to Lisa and Jean-Phillipe for their advices and support.

Por último, sin que el orden tenga importancia alguna, agradecer a mi familia su infinita paciencia.

Muchas gracias.

Rafa

Resum

Els beneficis clínics dels ultrasons (US) són coneguts desde fa molts anys. De fet, els US representen una tècnica de diagnostic mèdic mitjançant la imatge molt atractiva, degut a la seva seguretat, rapidesa, relatiu baix cost i versatilitat. A més a més, és una tècnica que no és agresiva pel pacient, a diferència d'altres mètodes, com els rajos X. A més a més, el seu emmagatzemament i la seva instal·lació són també més simples que en altres casos.

Encara que presenta una resolució bastant pobre, observadors experts poden fer anàlisis qualitatius per detectar malalties locals, tot i que en malalties difoses els resultats no són tan bons. Les enfermetats locals presenten diferènces en la formació de l'eco entre les zones sanes i les malaltes, peró en el cas de que sigui una malaltia difosa, l'òrgan sencer pot estar afectat de manera que no es puguin veure contrastos en la intensitat de l'eco per basar un diagnòstic. Diferenciar entre teixits normals i malalts és difícil i s'acostuma a basar en anàlisis arbitraris. Així doncs, un análisi quantitatiu de les imatges pot permetre una millor detecció d'aquestes malalties difoses.

La tasca desenvolupada en aquest projecte ha estat orientada a la creació d'una aplicació evaluadora del grau de qualitat, en temes de salut, del muscle encarregat de fer força al mastegar. L'estructura del classificador implementat es presenta a la figura 1.2. Per fer l'anàlisi, va ser necessari desenvolupar una eina per a la detecció del muscle dins la imatge. Degut a la naturalesa de les imatges, es va escollir un procés de detecció guiat per l'usuari, mitjançant la creació d'una funció de cost a minimitzar, emprant expressions difuses [1] i aplicant programació dinàmica per reduir el càlcul computacional. L'extracció de la informació va ser realizada analitzant les textures dels muscles. Degut a que els elements a análitzar eren petits i que les imatges presenten molt soroll en forma de taques, representant falsos ecos, un anàlisi estadístic es va dur a terme. En concret els algoritmes desenvolupats van ser: les matrius de co-occurrència i les mesures d'energia d'una textura de Laws.

[1] fuzzy expressions

Un altre problema va ser la selecció de la informació a analitzar d'entre tot el conjunt de característiques extretes de cada imatge, degut a que moltes d'aquestes característiques no contenen informació vàlida per a una correcta classificació. Aquesta selecció es va realitzar amb una combinació de diverses tècniques: *sequential forward selection*[2], *cross-validation*[3] i minimització de l'error quadràtic mig. Com qualsevol altre classificador, va ser necessari un procés d'entrenament per tal de garantir el seu correcte funcionament. Cal dir que el procés de selecció i el d'entrenament es van dur a terme simultàniament, degut a què tots dos processos estan íntimament lligats.

El capítol 2 presenta informació detallada sobre la detecció del muscle mitjançant la detecció dels seus marges. El capítol 3 presenta una visió global sobre textures. A més a més, profunditza en les tècniques d'anàlisi de textures, particularitzant en les tècniques estadístiques i, en més en concret, en les dues tècniques emprades. El capítol 4 , es centra en la selecció de les característiques, en el procés d'entrenament i en els resultats obtinguts.

[2] selecció cap endavant seqüencial

[3] validaci'øcreuada

Contents

List of Figures

Chapter 1

Introduction

1.1 State of the art

The clinical benefits of ultrasound (US) have been known for many years. US is an attractive diagnostic medical imaging technique because its safety, speed, relative low cost, and versatility. Unlike such methods as X-rays, Computed Axial Tomography Scan (CAT-SCAN), cameras sensitive to radioactive material, and other methods which obtain images of sections of the human body and are invasive due to radioactivity, US is noninvasive. The fact that US is noninvasive allows the medical doctor to obtain several images of the part of the body which is of particular interest, and no special precaution measures have to be taken. Moreover, the logistics of storage and installation of ultrasound machines are easier than the CAT-SCAN, X-rays, and others, since US machines are smaller and lighter.

Despite its relatively poor resolution, qualitative evaluation of US images by human experienced observers is a reliable tool for the detection of focal diseases in several organs (for example, the liver), while in the case of diffuse diseases the results are less promising. Focal diseases can be identified by differences in echogenicity between normal and diseased areas, while in the presence of diffuse disease, the entire organ can be affected, so there is no contrast in echo intensity on which to base a diagnosis. Visually distinguishing normal tissue from diseased tissue is a difficult task. This has led to the use of quantitative analysis of US signal as a means of detecting diffuse diseases.

1.1.1 Ultrasonography

In US, the produced sound signal is directed via a probe to a section of the body. A part of the signal is absorbed, another part of it is reflected back directly, and the other part of it bounces onto one or more points before it is reflected back to the receiver. Due to the multiple reflections of the sound signal (scattering of the signal), significant noise is incorporated with the signal. The received sound intensity is quantized usually on a gray scale between 0 and 255 and therefore transformed from the sound space to the image space, and it is in the image space that we operate. The US signal is absorbed differently by the various parts of the body. Thus, soft tissue reflects signal differently than muscle, or bone.

All the images used in this project are a cross-sectional view from the skin (at the top) through the muscle to the bone (at the bottom), as can be seen in figure 1.1. Tendons are seen as white structures, which look like lines in a chestnut leaf. The intramuscular echo intensity reflects the amount of muscle mass: when the structures around tendons are seen as black, it means that there is a lot of muscle mass, which is a good sign. The ramus is seen in the bottom of the image as a white line more or less wide. This is the image of the bone. The ramus bone is seen quite distinctly on all the copied images whether tendons and the muscle mass (echo intensity) is seen in varying quality.

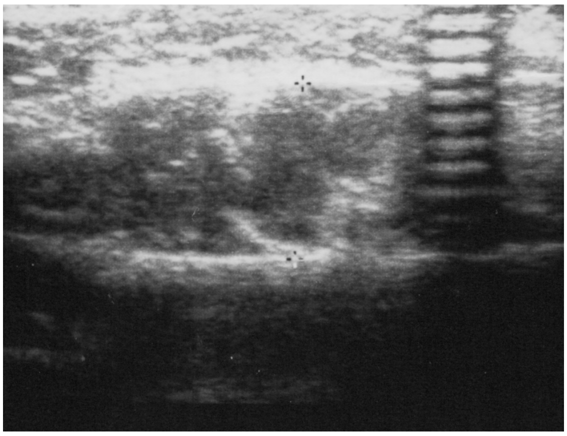

Figure 1.1: US image description

1.2 Materials and methods

This project has been developed in cooperation with Dept. of Orthodonthy at the University of Geneva. The aim of this project was to define a method to evaluate objectively the quality of the masseter muscle, which was determined by Stavros Kiliaridis, PhD[1], in a four-point scale. Thus, the task is to classify an unknown texture into one of the known classes, using the information extracted from the training images. The texture classification problem is conventionally divided into two sub-problems, that is, feature extraction and the classification with the computed features (see figure 1.2). Moreover, feature extraction part has an additional problem: feature selection, that is, to decide which features of the starting set must be extracted to get the maximum information and, at the same time, avoid adding features which have no useful information.

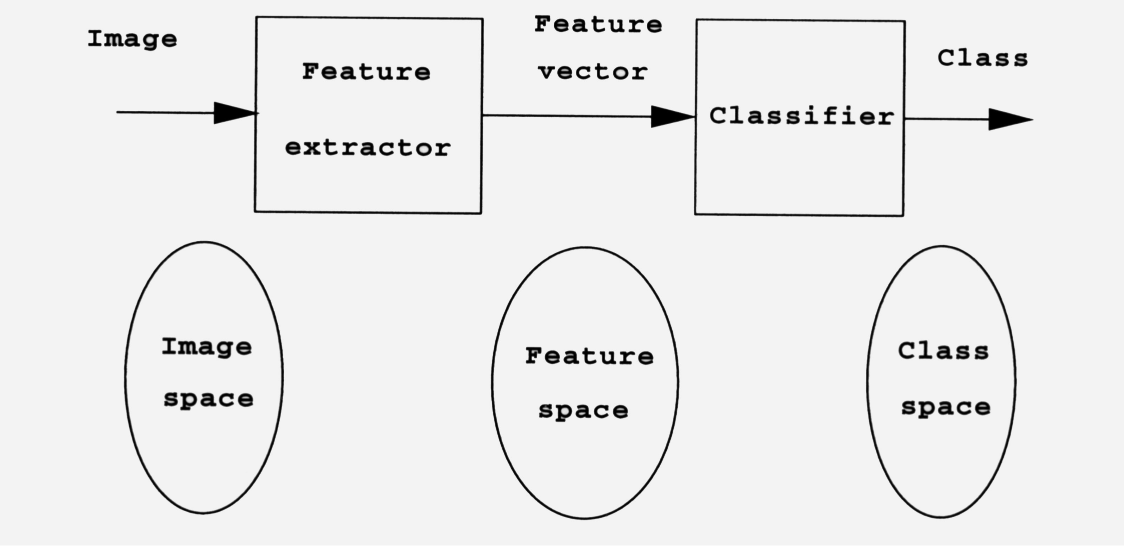

Figure 1.2: Classification system structure

All patients were examined with US imaging of masseter muscles with a real-time scanner (*Acuson*, Acuson Corporation, Mountain View, CA, USA). The real-time scans were printed on film paper by a videocopy printer (*Mitsubischi*, model PGGE, Mitsubischi Electric Corporation, Osaka, Japan). For all subjects and conditions the imaging were performed twice, a total of eight images per subject. Previously, all these images were used to evaluate

[1] Professor and Chairman, Department of Orthodontics. University of Geneva, Genève, Switzerland

the influence of the masseter muscle on the shape, thickness, bone mass and trabeculation of the mandibular alveolar process. These images were scanned to perform the analysis with a scanner (*Epson*,model Perfection 1200, Seiko Epson Corporation, Seoul, Republic of Korea), with a resolution of 300*300 dpi. Image set was composed by 361 images, distributed as follows: 32 images of class 1, 81 of class 2, 136 of class 3 and 112 of class 4.

Image processing methods hold the potential to provide objective and quantitative measures of US images. Previous studies by other groups have identified texture analysis as being useful in the analysis of US images[1, 2, 3].

1.3 Organization

Chapter 2 presents how the muscle borders were found. A complete explanation of the algorithm can be found, detailing information about subtechiques that have been used, such as fuzzy expressions. Qualitative results are shown. Chapter 3 shows an introduction to texture analysis, as a feature extraction technique. A description of co-occurrence matrices and Laws energy measures algorithms will be presented. Chapter 4 focuses on feature selection and on classifier construction, and then results are presented and discussed.

Chapter 2

Boundary Detection

Due to scattering and speckle noise, the shape of a border profile in a US image can vary significantly. Finding maximal gradient points is an initial approach to the problem, but it does not work because it doesn't takes into account the connectivity of the boundary. Therefore, it is necessary to find other mechanisms as well as ways of implementing them in a computer-based algorithm. Hence, the boundary detection system used in this project was based in other systems already developed for more difficult cases, as the boundary detection problem in US artery images [4, 5, 6]. Researchers in this area propose a global approach to boundary detection. This global analysis is performed via the definition of a cost function containing information about image features, which try to fit to human perception. Usually, human perception works with really imprecise information. This imprecision can be modeled with fuzzy expressions. Finally, human intervention can be useful in two ways: as an a priori knowledge, it can be used to train the system; as a posteriori knowledge, it can be used to solve ambiguous cases by direct human assistance and including this information as a cost term in the cost function.

2.1 Fuzzy Expressions

A fuzzy expression is a tool to mimic human global perception, which is not linear. For example, human hearing doesn't respond linearly to sound activity; it does it logarithmically. So it is corrupting the input information. That's what fuzzy expressions do. Therefore, they transform a rigid criterion, such as gradient or brightness, to a relaxed criterion that provides orientative information. Thus, instead of using directly a feature value $f(p)$ in the cost function, where p is a pixel, a fuzzy expression $\mu(\cdot)$ is applied to the feature value, so the cost function weights the fuzzy expression of the pixel feature $\mu(f(p))$. For example, an expert observer wouldn't consider faint echoes to decide where are the borders. Besides, if an echo has certain brightness, the expert will give it the same importance as other brighter echoes. In figure 2.1(a), we can see an example of this expert's interpretation of an image feature in a fuzzy function called $\mu 1_a(\cdot)$. Figure 2.1(b) shows another fuzzy function (we have called it $\mu 2_a(\cdot)$) those functions in the opposite way. The thresholds were calculated empirically.

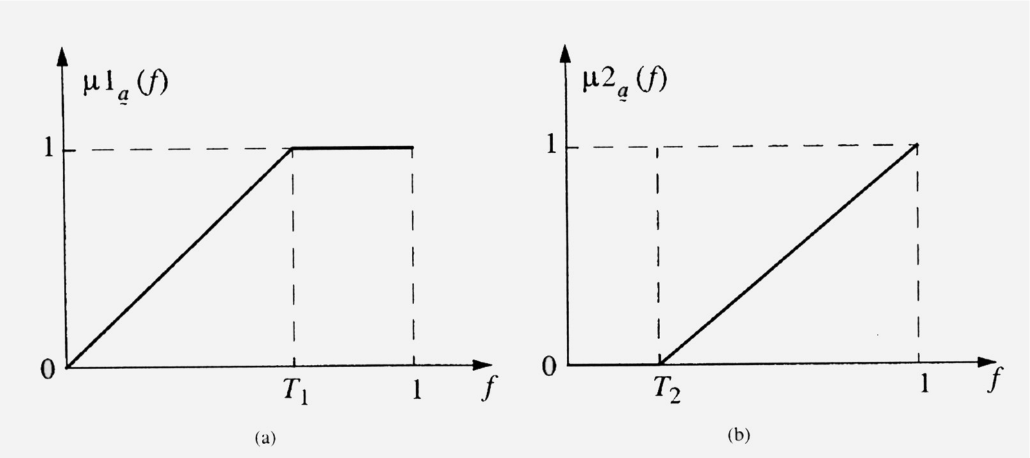

Figure 2.1: Two types of fuzzy expressions

2.2 Cost Function and Cost Terms

The construction of a cost function that matches human perception as a full-automatic system is really hard to reach in US images. Instead, an MxN region is considered, and a full analysis over this area is performed. Thus, taking this area as a grid, we consider a deformable polyline B_N that contains N nodes, one in each column and each column composed by M candidates, so we can denote B_N as $B_N = \{p_1, p_2, \ldots, p_N\}$, where p_i can be anyone of the M candidates. The cost function can be labeled as $C(B_N)$, and is defined as a sum of the local costs along a candidate boundary for the polyline B_N

$$C(B_N) = c_F(p_1) + \sum_{i=2}^{N} (c_F(p_i) + c_G(p_{i-1}, p_i)) \tag{2.1}$$

where local costs are composed by

$$\begin{aligned} c_F(p_i) &= \sum_{j=1}^{K} w_i \tilde{f}_j(p_i) \qquad (i = 1, \ldots, N) && (2.2) \\ c_G(p_{i-1}, p_i) &= w_{k+1} g_j(p_{i-1}, p_i) \qquad (i = 2, \ldots, N) && (2.3) \end{aligned}$$

in which $\tilde{f}_j(p_i)(j = 1, \ldots, K)$ are image feature terms, K is the number of features used. The term c_F refers to the cost associated with the computed features and c_G is related to geometric costs. We write $\tilde{f}_j(p_i)$ because they are transformations of image feature values $f_j(p_i)$ with fuzzy expressions. If we want every weight to be positive, we must define $\tilde{f}_j(p_i)$ so that a high feature value at p_i will result in a low $\tilde{f}_j(p_i)$ value, hence, a low local cost that will attract the polyline. The term $g(p_{i-1}, p_i)$ is called smoothness term, because it takes in account vertical distance between two consecutive points p_i and p_{i-1}. Higher vertical distances will result in higher vertical values and hence, a higher local cost will punish the connection between these two points. It's called smoothness term because it tries to keep the line smoother. Hence, the resulting boundary $\widehat{B_N}$ is the optimal B_N that minimizes $C(B_N)$

$$\widehat{B}_N = \{B_N \mid min(C(B_N))\} \tag{2.4}$$

2.3 Dynamic Programming

Normally, the local-cost surface around the boundary that we are looking for is not convex in a real image. This convexity appears severely distorted, mainly in noisy images, such as US images. All the searching space must be analyzed to avoid locking the solution in a local minimum. A straightforward exhaustive search is necessary to succeed in finding the right solution, but it is necessary to rewrite 2.1 to reduce the computational complexity from an order of M^N in terms of cost function evaluations. This can be solved by defining 2.1 as a recursive expression:

$$\begin{aligned} C(p_1, 1) &= c_F(p_1) \qquad (n = 1) \\ C(p_1, p_2, \ldots, p_n, n) &= c_F(p_1) \\ &+ \left\{ \sum_{i=2}^{n-1} (c_F(p_i) + c_G(p_{i-1}, p_i)) \right\} \\ &+ \{c_F(p_n) + c_G(p_{n-1}, p_n)\} \end{aligned}$$

$$\begin{aligned} &= C(p_1, p_2, \ldots, p_{n-1}, n-1) \\ &+ (c_F(p_n) + c_G(p_{n-1}, p_n)) \\ &\qquad (n = 2, \ldots, N) \end{aligned} \tag{2.5}$$

Applying 2.5 instead of 2.1 the computational complexity is reduced to an order of NxM^2. To satisfy 2.4, we consider the candidate minima as a cost function of the last node of $B_N(p_n)$:

$$\tilde{C}(p_n, n) = min_{p1,\ldots,p_n}\{C(p_1, p_2, \ldots, p_n, n)\} \tag{2.6}$$

If 2.5 is applied over 2.6, we can express it as a cost accumulation process

$$\begin{aligned} \tilde{C}(p_1, 1) &= c_F(p_1) \qquad (n = 1) \\ \tilde{C}(p_1, p_2, \ldots, p_n, n) &= min_{p1,\ldots,p_{n-1}}\{C(p_1, p_2, \ldots, p_{n-1}, n-1) \\ &+ (c_F(p_n) + c_G(p_{n-1}, p_n))\} \\ &= \tilde{C}(p_1, p_2, \ldots, p_{n-1}, n-1) + (c_F(p_n) + c_G(p_{n-1}, p_n)) \\ &\qquad (n = 2, \ldots, N) \end{aligned} \tag{2.7}$$

Accumulating costs according to 2.7, at each stage n, the location of p_{n-1} that defines $\tilde{C}(p_n, n)$, as expressed in 2.7, is recorded for each instance of p_n. Hence, the nodes of the optimal boundary $\widehat{B}_N$ defined in 2.4 can be found by backtracking.

$$\widehat{P}_N = (p_N \mid C(p_1, p_2, \ldots, p_N) = min_{p_N}\tilde{C}(p_N, N)) \tag{2.8}$$

$$\begin{aligned} \widehat{P}_{n-1} &= (p_{n-1} \mid min_{n-1}\{\tilde{C}(p_{n-1}, n-1) \\ &+ (c_F(\widehat{P}_n) + c_G(p_{n-1}, \widehat{P}_n))\}) \qquad (n = N, \ldots, 2) \end{aligned} \tag{2.9}$$

where $\widehat{P}_N$ refers to the selected point for p_N (the last node) and $\widehat{P}_{n-1}$ refers to the selected points for the rest of the nodes.

2.4 Human Intervention

A human intervention mechanism becomes necessary when obvious errors are detected. This method suggests adding human intervention as a member of the cost function. This human intervention is introduced into the cost function as an external force term defined as

$$c_E(p_k, q_k) = w_e d^2(p_k, q_k). \tag{2.10}$$

It is a monotonously increasing function of the distance d between the candidate node p_k and the manually set point q_k that has been inserted in the kth column. Due to the smoothness, just one punctual setting has a global effect over the whole trajectory of the boundary. The w_e weight decides the attraction strength force. Thus, the initial definition of the cost function (2.1) becomes

$$\begin{aligned} C(B_N) &= c_F(p_1) + \sum_{i=2}^{N} \{(c_F(p_i) + c_G(p_{i-1}, p_i)) \\ &+ \sum_{l=1}^{Q} \delta(i - k_l) c_E(p_i, q_{k_l})\} \qquad (2.11) \end{aligned}$$

where Q is the number of user-set points $(q_{k_1}, q_{k_2}, \ldots, q_{k_Q})$ and $\delta(n)$ ensures that an extra term $c_E(\cdot)$ is added only to the nodes that are in the columns that have human-set points.

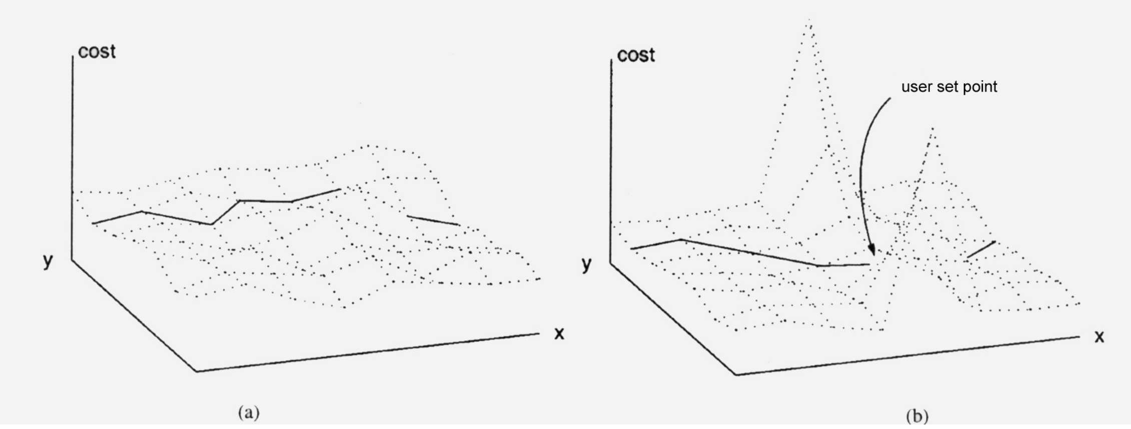

Figure 2.2: Human intervention effect in the cost function. Left figure shows the cost function without any user points. A U-shaped gap appears centered in where the point has been placed. Hence, the shape of the gap pushes the boundary toward the point.

Figure 2.2 shows how this mechanism affects to cost function. The solid line represents the detected border passing through the local cost surface. This path is determined following the surface valley and, at the same time, minimizing the curvature. Without any point set by the user (figure 2.2(a)), the border has a different form than after setting one point (figure 2.2(b)). A local U-shaped gap appears centered in the column where the point has been set, forcing the border to modify its form from the original one. It is important to notice that setting a point to modify the detected boundary does not mean that the boundary will pass through this point. It just means that the boundary will be pulled toward this point.

2.5 Implementation and Results

Three terms composed the cost function:

- Boundary smoothness: this term evaluated the number of rows that separated two points p_{i-1} and p_i:

  $$g(p_{i-1}, p_i) = (p_{i-1_y} - p_{i_y})^2$$

- Gradient value: lower values of gradient were punished. This term was filtered with a fuzzy expression: $\mu 1_a(\cdot)$, as defined in figure 2.1(a). This gradient was computed with a 5 x 5 neighborhood and normalized. It is also fitted to the intensity values within this window. The threshold used in the fuzzy expression $\mu 1_a(\cdot)$ was $T_1 = 0.4$.

- User-set points: as told previously, this term punishes with the square of the number of rows that a candidate point p_i is far from a user-set point in this same column i. A little modification has been added to for a higher attraction: a users-set point affects to its column and to the previous and following column, but in these cases with less intensity (half intensity).

An improvement of the explained procedure has been applied in terms of computing cost. Just a part of the image was analyzed when searching skin and bone border, but additionally, for each analyzed point a little part of the analyzed region was taken into account, reducing the cases to analyze, and hence reducing the time expense.

No qualitative results have been computed, but figures 2.3, 2.4 and 2.5 are some examples of its functionality.

Figure 2.3 is a typical example of the human intervention effect over the resulting skin border. Figure 2.3(a) shows the original image, and figure shows the resulting border with only gradient and geometrical costs computed. This border has been bad calculated because other echoes, which presented high gradient values, were enough close to become a candidate border, and finally the system has selected it (figure 2.3(b)). Two points were added by the user to attract the border (figure 2.3(c)): the left one to avoid the three first echoes that appear almost aligned and are close to the starting point. The second one to avoid the white cloud close to the ending point that, because of its irregularity, it could be interpreted as the border. Just with these two points the border fits correctly.

Figure 2.4 shows an example of a skin border that the system could find correctly without human intervention. The original image (figure 2.4(a)) does not present strong echoes grouped, and it just appears a white cloud quite regular near the starting point. In this case, the geometrical term is enough to correct any possibility of selecting another possible candidate border (figure 2.4(b)).

Normally, skin borders are more difficult to detect than the bone borders because of tendinous structures (white clouds) that fall from the skin border. The bone border is usually quite clear. In these cases no human intervention is needed. An example is shown in figure 2.5(a). However, sometimes some noise appears in the nearby of the bone border (figure 2.5(b)) and human intervention is needed to avoid analyzing bone border points, if echoes are below the bone border, or to maximize the analyzed area, if echoes are above the bone border (figure 2.5(c)). Moreover, in section 4, muscle height and width are used to decide muscle class, so it is important to correct this possible mistakes.

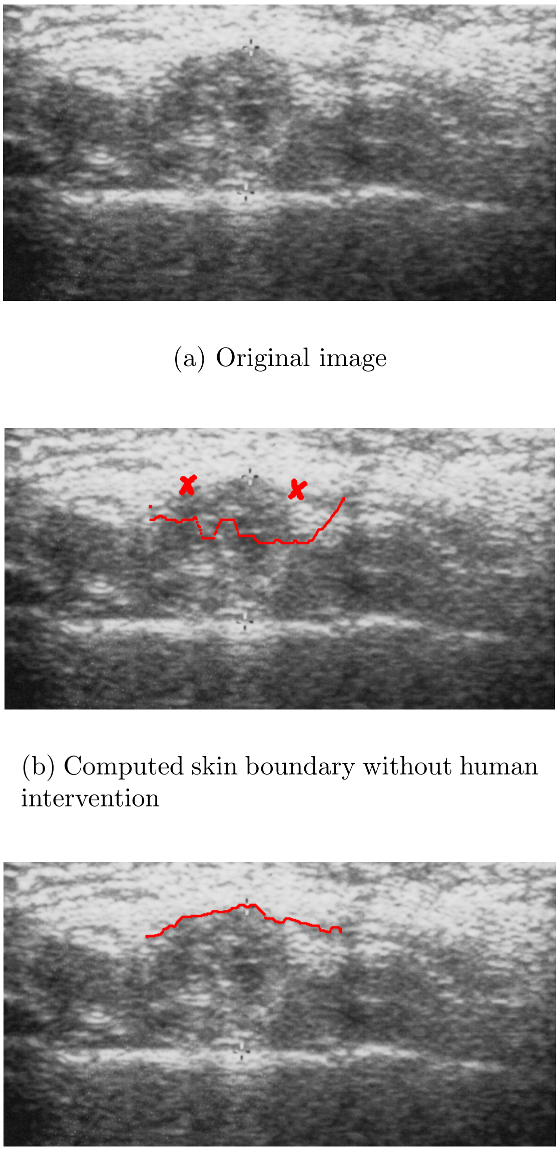

(a) Original image

(b) Computed skin boundary without human intervention

(c) Computed skin boundary with human intervention

Figure 2.3: Skin border where human intervention is needed

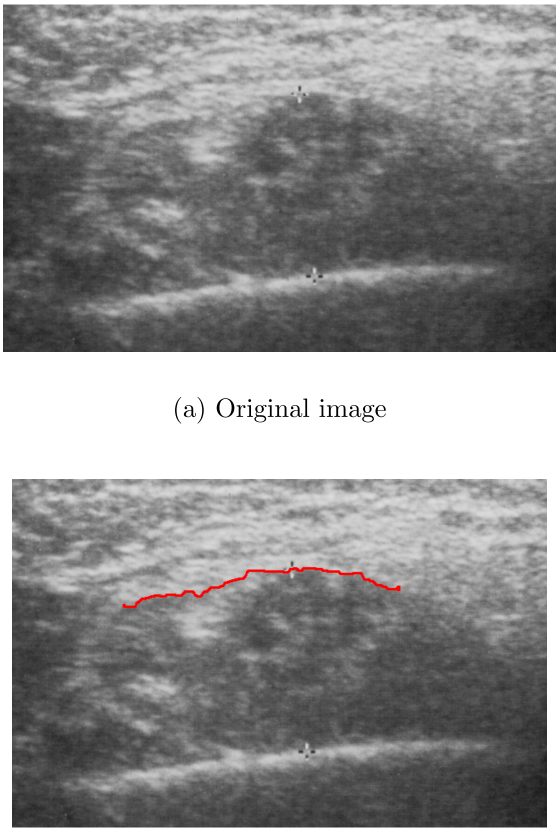

(a) Original image

(b) Computed skin boundary without human intervention

Figure 2.4: Skin border where no human intervention is needed

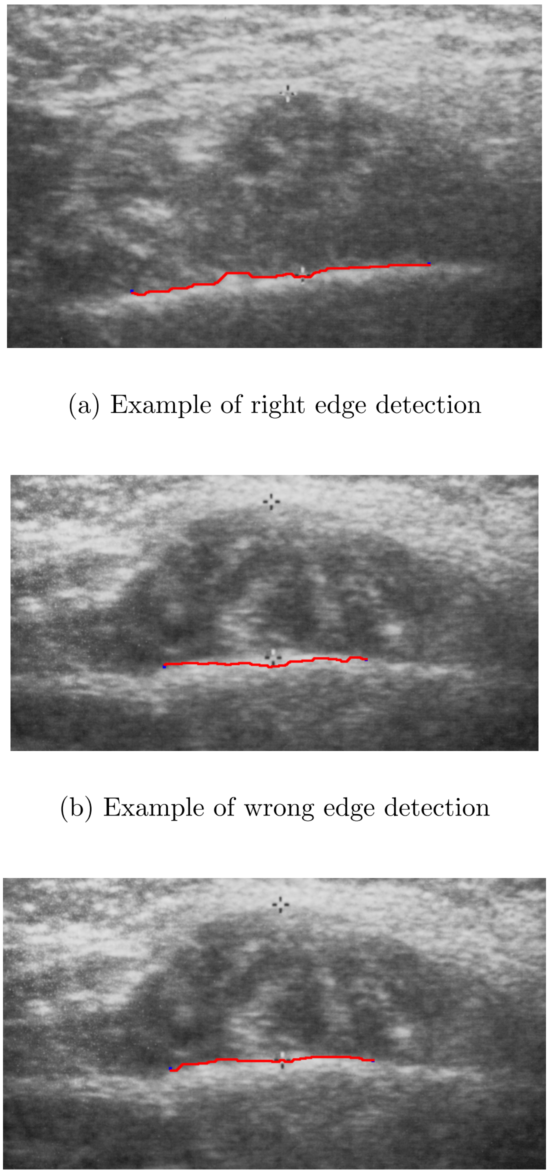

(a) Example of right edge detection

(b) Example of wrong edge detection

(c) Bad edge detection corrected with human intervention

Figure 2.5: Bone border computation examples

Chapter 3

Textures

3.1 What is a Texture?

Many papers on texture analysis begin with stating that there exists no precise definition of Texture. Others don't give any definition or give a definition that suits to the method that they present. The intuitive nature of the term can be a reason and, moreover, it becomes really hard to capture these imprecisions in a concrete definition. Anyway, some definitions have been presented in image processing handbooks and texture papers. Some examples can be found in [7, 8, 9, 10, 11, 12].

Even with this difficulty to get a definition, texture is a term widely used and well understood in common language. The term is usually used to describe intrinsic properties of an object, such as granulation, roughness, coarseness, etc. So it could be defined as *something consisting in mutually related elements*, or more formally, *a set of local neighborhood properties*. Hence, it can be stated that when we talk about textures we are considering a group of pixels, sometimes called texture primitive or texture element, and the texture described is highly dependent on the number of pixels considered (the texture scale)[13]; texture description is scale dependent.

3.2 Texture Analysis

3.2.1 Introduction

The main aim of texture analysis is texture recognition and texture-based shape analysis. Such features can be found in the tone (brightness in gray-level images) and in the structure of a texture[13]. Tone is mostly a single pixel feature. Besides, structure is the relationship between them but, however, tone and structure are not independent. Figure 3.1 shows an example: figures 3.1(a) and 3.1(b) have the same number and type of elements, but they don't have the same texture; besides, figures 3.1(a) and 3.1(c) have the same spatial relationship of elements, but again they show different textures.

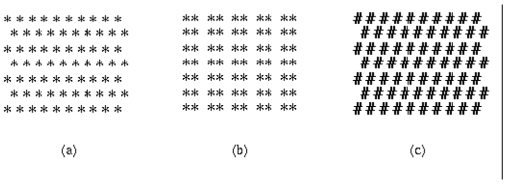

Figure 3.1: Textures with tonal or structural similarities

3.2.2 Utility

Texture analysis plays an important roll in areas such as scene analysis, medical image analysis, remote sensing and other application areas. Texture analysis is used in the following tasks:

- the *classification* of images based on their textural appearance (this project is an example of this tasks);
- the *segmentation* of images into regions, which have similar textural properties;
- other *information extraction* from textural cues, e.g. for reconstructing 3D scenes from 2D scenes.

Image classification is the basic task that deals with associating images as a whole with classes from a predefined set. Image segmentation is a localized version of image classification, because every pixel of an image is classified individually or in small groups.

3.2.3 Texture Analysis Techniques

Several texture analysis techniques exist, but two main texture description approaches can be identified: *statistical* and *syntactic*[13].

Statistical methods gather information about textures exploiting pixels statistics: this can be first order statistics, such as mean and variance, but more importantly higher order statistics, mostly second order. These methods compute different properties, such as directionality or periodicity, and are suitable if texture elements sizes are comparable with the pixel sizes.

Syntactic and *hybrid* methods (combination of statistical and syntactical methods) are more suitable where texture elements can be assigned a label (their type). In these cases, texture elements can be described not only using tonal properties, but also using a larger variety of them.

From now on, syntactical methods are let aside in favor of statistical methods, which have been used in our system. This selection has been done because texture elements are comparable with the pixel size, so statistical methods fit better than the syntactical methods. Additionally, previous research projects have shown statistical texture analysis to fit well to US images [14, 15, 16].

3.2.4 Statistical Methods

Several statistical texture analysis methods have been described, such as:

- *autocorrelation texture description*, which is based on spatial frequencies, describing their organization by a correlation coefficient that evaluates linear spatial relationships between texture elements. A single pixel is considered as a texture element and its tone property is the gray-level;
- *co-occurrence matrices* method of texture description is based on the repeated occurrence of some gray-level configuration in the texture (see section 3.3);
- *edge frequency* method is obviously based in edge detection with any edge detector for different distances (texture is scale dependent, 3.1);
- *primitive run length* method is based in catching a large number of constant-gray-levels pixels in a located line;
- *Laws' texture energy measures* method is based in determining texture properties by assessing average gray-level, edges, spots, ripples and waves in texture(see section 3.4);

- *fractal texture description* is based in correlation between texture coarseness and fractal dimension of a texture, as demonstrated in [17].

3.3 Co-occurrence Matrices

The co-occurrence matrices method of texture description, also called Haralick's method and spatial gray-level dependency matrices, is a second-order statistical approach. It is based on the repeated occurrence of some gray-level configuration in the texture. Textural features are derived from angular nearest-neighbor spatial-dependence matrices[18]. This method has become one of the most well known and it is widely used for texture description.

A co-occurrence matrix is the joint probability of occurrence of gray levels i and j for two pixels with a defined spatial relationship in an image. This spatial relationship is defined in terms of distance d and orientation ϕ.

Let D be the part of an image to be analyzed which size is MxN. An occurrence of some gray-level configuration can be described as a matrix of relative frequencies $P_{\phi,d}(a,b)$, representing the number of times two pixels with gray-levels a and b occur in D separated by a distance d and orientation θ, from each other. These matrices are not symmetric, but usually are defined as $P_{\phi,d}(a,b) = P_{\phi,d}(a,b) + P_{\phi,-d}(a,b)$, resulting a formulation as shown below, to avoid this asymmetry and reducing the number of matrices to compute from 8 to 4. Hence, non-normalized definitions of co-occurrence as functions of angle and distance can be represented formally as

$$\begin{aligned}
P_{0^\circ,d}(a,b) &= \mid \{\{(k,l),(m,n)\} \in D : \\
&\quad k-m=0, \mid l-n \mid= d, f(k,l)=a, f(m,n)=b\} \mid \\
P_{45^\circ,d}(a,b) &= \mid \{\{(k,l),(m,n)\} \in D : \\
&\quad (k-m=d, l-n=-d) OR (k-m=-d, l-n=d), \\
&\quad f(k,l)=a, f(m,n)=b\} \mid \\
P_{90^\circ,d}(a,b) &= \mid \{\{(k,l),(m,n)\} \in D : \\
&\quad \mid k-m \mid= d, l-n=0, f(k,l)=a, f(m,n)=b \quad \mid \\
P_{135^\circ,d}(a,b) &= \mid \{\{(k,l),(m,n)\} \in D : \\
&\quad (k-m=d, l-n=d) OR (k-m=-d, l-n=-d), \\
&\quad f(k,l)=a, f(m,n)=b\} \mid \qquad (3.1)
\end{aligned}$$

where $| \{\ldots\} |$ refers to set cardinality.

As an example, let's consider the following 4x4 image containing 3 different gray values:

$$\begin{matrix} 1 & 1 & 0 & 0 \\ 1 & 1 & 0 & 0 \\ 0 & 0 & 2 & 2 \\ 0 & 0 & 2 & 2 \end{matrix}$$

The 3x3 gray-level co-occurrence matrices for this image for orientations $\theta = 90^o$ and $\theta = 135^o$ and distance $d = 1$ are given below:

$$P_{90^o,1} = \begin{bmatrix} 8 & 2 & 2 \\ 2 & 4 & 0 \\ 2 & 0 & 4 \end{bmatrix} \qquad P_{135^o,1} = \begin{bmatrix} 4 & 2 & 2 \\ 2 & 2 & 1 \\ 2 & 1 & 2 \end{bmatrix}$$

The element $P_{90^o,1}(0,2)$ represents the number of times two pixels with gray-levels 0 and 2 and separated by distance 1 appear in direction 90^o: $P_{90^o,1}(0,2) = 2$. Similarly, $P_{135^o,1}(2,1)$ counts the number of appearances of two pixels with gray-levels 2 and 1, separated by distance 1; so $P_{135^o,1}(2,1) = 1$. The rest of matrices are built in the same way.

If the texture is coarse and distance d is small compared to the size of the texture elements, the pairs of points at distance d should have similar gray levels. Inversely, for a fine texture, if distance d is comparable to the texture size, then the gray levels of points separated by distance d should often be quite different, so that values in the co-occurrence matrix should be spread out relatively uniformly. Therefore, a good way to analyze texture coarseness would be, for various values of distance d, some measure of scatter of the matrix around the main diagonal. Similarly, if the texture has some direction (coarser in one direction than another) then the degree of spread of the values about the main diagonal in the matrix should vary with the direction d.

Haralick proposed some texture features to be extracted from co-occurrence matrices. Different authors have used them with different names, so it is better just keep in mind that these features take information to form a classification criteria.

3.4 Laws' Texture Energy Measures

Certain gradient operators such as Laplacian and Sobel operators remark the underlying microstructure of texture within an image. This method is based in a similar principle. It uses series of pixel impulse response arrays obtained from combinations of one-dimensional vectors[19]. These vectors are derived from three base vectors

$$L_3 = (1, 2, 1) \qquad E_3 = (-1, 0, 1) \qquad S_3 = (-1, 2, -1) \tag{3.2}$$

which represents, respectively, averaging (level), first difference (edges) and second difference (spots). If it is necessary to obtain longer vectors to analyze an image in different scales, a convolution of these vectors with themselves and each other must be applied until we obtain the desired length. After first convolution, five vectors result

$$\begin{aligned} L_5 &= (1, 4, 6, 4, 1) \\ E_5 &= (-1, -2, 0, 2, 1) \\ S_5 &= (-1, 0, 2, 0, -1) \\ R_5 &= (1, -4, 6, -4, 1) \\ W_5 &= (-1, 2, 0, -2, 1) \end{aligned} \tag{3.3}$$

which are associated to and underlying microstructure and labeled with acronyms accordingly (L to Level, E to Edge, S to Spot, W to Wave and R to Ripple).

The two-dimensional convolutional kernels (named 5x5 Laws' masks) resulted from multiplying these length-five vectors, by transposing the first vector term and leaving the second term as a row vector. They are applied to the digital image to get the measures, and then a nonlinear windowing operation is performed. After this convolution, we obtain 25 different two-dimensional convolutional kernels. As an example the L5E5 kernel is found by convolving L5 vector with the E5 vector. A listing of all 5x5 kernel names is given below:

L5L5	E5L5	S5L5	W5L5	R5L5
L5E5	E5E5	S5E5	W5E5	R5E5
L5S5	E5S5	S5S5	W5S5	R5S5
L5W5	E5W5	S5W5	W5W5	R5W5
L5R5	E5R5	S5R5	W5R5	R5R5

The next step is dedicated to explain how to compute the texture energy measures over a digital image.

3.4.1 Laws Algorithm

Let D be a NxM digital image that we want to analyze with regards to its texture properties. We first apply each of the 25 convolutional kernels to the image, resulting in a set of 25 NxM gray-level images, which will be the basis for the textural analysis. Next, we replace every pixel in the 25 NxM separate grayscale images with Texture Energy Measure (TEM) at the pixel. We do that by applying a nonlinear windowing to the set of 25 NxM images, resulting a new set of 25 NxM images, which we will refer to as TEM images. Laws suggest two nonlinear filters:

$$\mathrm{TEM}(x,y) = \sum_{i=-5}^{5}\sum_{j=-5}^{5} \mid \mathrm{BaseImage}(x+i,y+j) \mid \tag{3.4}$$

$$\mathrm{TEM}(x,y) = \sqrt{\sum_{i=-5}^{5}\sum_{j=-5}^{5} \mathrm{BaseImage}^2(x+i,y+j)} \tag{3.5}$$

At this point, again, we have 25 new images (TEM images) that we will name with the original convolution kernels with an appended ”T”, to indicate that they are texture energy measures and to make any reference to them easier. Thus, the TEM images are named as follows:

L5L5T	E5L5T	S5L5T	W5L5T	R5L5T
L5E5T	E5E5T	S5E5T	W5E5T	R5E5T
L5S5T	E5S5T	S5S5T	W5S5T	R5S5T
L5W5T	E5W5T	S5W5T	W5W5T	R5W5T
L5R5T	E5R5T	S5R5T	W5R5T	R5R5T

In some applications, texture directionality is not important. In this case, similar features can be combined to remove directional information. For example, while L5E5 is sensitive to vertical edges, E5L5 is sensitive to horizontal edges. Adding these TEM images, we have a new single feature sensitive to ”edge content” in a general sense. If we want to work with these ”general-sense” features, TEM images generated with transposed convolution kernels are added together. Lets denote these new images with an appended ”R” meaning ”rotational invariance”. We will call this images TR images.

$$\begin{array}{lllll}
\mathrm{E5L5TR} & = & \mathrm{E5L5T} & + & \mathrm{L5E5T} \\
\mathrm{S5L5TR} & = & \mathrm{S5L5T} & + & \mathrm{L5S5T} \\
\mathrm{W5L5TR} & = & \mathrm{W5L5T} & + & \mathrm{L5W5T} \\
\mathrm{R5L5TR} & = & \mathrm{R5L5T} & + & \mathrm{L5R5T} \\
\mathrm{S5E5TR} & = & \mathrm{S5E5T} & + & \mathrm{E5S5T} \\
\mathrm{W5E5TR} & = & \mathrm{W5E5T} & + & \mathrm{E5W5T} \\
\mathrm{R5E5TR} & = & \mathrm{R5E5T} & + & \mathrm{E5R5T} \\
\mathrm{W5S5TR} & = & \mathrm{W5S5T} & + & \mathrm{S5W5T} \\
\mathrm{R5S5TR} & = & \mathrm{R5S5T} & + & \mathrm{S5R5T} \\
\mathrm{R5W5TR} & = & \mathrm{R5W5T} & + & \mathrm{W5R5T}
\end{array}$$

There are five remaining cases, which are scaled by 2 to keep all features consistent.

$$\begin{array}{lllll}
\mathrm{E5E5TR} & = & \mathrm{E5E5T} & * & 2 \\
\mathrm{S5S5TR} & = & \mathrm{S5S5T} & * & 2 \\
\mathrm{W5W5TR} & = & \mathrm{W5W5T} & * & 2 \\
\mathrm{R5R5TR} & = & \mathrm{R5R5T} & * & 2 \\
\mathrm{L5L5TR} & = & \mathrm{L5L5T} & * & 2
\end{array}$$

L5L5T is usually discarded when no contrast information is needed, and this information is used to scale the other TEM images pixel by pixel. At this point we have a set of 15 texture features (14, when L5L5T is discarded), which are rotational invariant. Another possibility is keeping directional information and work with a set of 25 TEM images, which will be the texture feature set. Whatever the process followed, at this point, we get a data set where every pixel is represented by M texture features, where M can be 14, 15 or 25, depending on which process was applied. Another step can be applied to get more information. It is possible to apply a statistical analysis over the remaining images (texture features) to get information about the distribution of these images. Thus, if we have M remaining images and we get N statistical values from each one, we finally get MxN statistical texture features from the original images.

3.5 Implementation and Results

In this chapter, both algorithm implementations are commented and extracted features are presented. Additionally, some images samples are presented of resulting co-occurrence matrices and Laws TR images.

Co-occurrence matrices

Several features were computed in both co-occurrence matrices and Laws methods.

For the co-occurrence matrix method, matrices were computed for distances 3, 5 and 7 and directions 0^o, 45^o, 90^o, 135^o and the all of them added, to find some rotational-invariant features. For each matrix, the following 11 features were computed[1]:

$$Energy = \sum_i \sum_j \mathrm{P}^2_{\phi,\mathrm{d}}(i,j) \tag{3.6}$$

$$Entropy = \sum_i \sum_j \mathrm{P}_{\phi,\mathrm{d}}(i,j) log_2(\mathrm{P}_{\phi,\mathrm{d}}(i,j)) \tag{3.7}$$

$$Contrast = \sum_i \sum_j (i-j)^2 \mathrm{P}_{\phi,\mathrm{d}}(i,j) \tag{3.8}$$

$$IDM = \sum_i \sum_j \frac{\mathrm{P}_{\phi,\mathrm{d}}(i,j)}{1+(i-j)^2} \tag{3.9}$$

$$Mean(\mu) = \sum_i i \sum_j \mathrm{P}_{\phi,\mathrm{d}}(i,j) \tag{3.10}$$

$$Standarddeviation(\sigma) = \sum_i (i-\mu)^2 \sum_j \mathrm{P}_{\phi,\mathrm{d}}(i,j) \tag{3.11}$$

$$correlation(\rho) = \sum_i \sum_j \frac{(i-\mu)(j-\mu)\mathrm{P}_{\phi,\mathrm{d}}(i,j)}{\sigma^2} \tag{3.12}$$

$$ClusterShade = \sum_i \sum_j ((i-\mu)+(j-\mu))^3 \mathrm{P}_{\phi,\mathrm{d}}(i,j) \tag{3.13}$$

$$ClusterProminence = \sum_i \sum_j ((i-\mu)+(j-\mu))^4 \mathrm{P}_{\phi,\mathrm{d}}(i,j) \tag{3.14}$$

$$DiagonalMoment = \sum_i \sum_j \frac{(\mid i-j \mid ((i-\mu)+(j-\mu))\mathrm{P}_{\phi,\mathrm{d}}(i,j)}{2(1+\rho)\sigma^2} \tag{3.15}$$

[1] both μ and σ correspond to μ_x and σ_x each, but they have the same value as μ_y and σ_y when working with symmetric matrices, so lets call them just μ and σ. Thus, every equation that contained this values have been redefined accordingly

$$SumCorrelation = \sum_i \sum_j \frac{(i-\mu)(j-\mu)((i-\mu)+(j-\mu))\mathrm{P}_{\phi,\mathrm{d}}(i,j)}{\sigma^3\sqrt{2(1+\rho)}} \quad (3.16)$$

Some of these features are quite well known, such as energy, entropy, mean, standard deviation or correlation. For the others, an explanation is presented:

- *Contrast* is a measure of local image variations.
- *IDM* (Inverse Different Moment) is a measure of the uniformity of an image: homogeneous images are represented with high values, and heterogeneous ones are represented by low values.
- *Cluster Shade* is a 2-D version of the gray-level histogram skewness. Skewness measures the degree of asymmetry of a distribution.
- *Cluster Prominence* is a 2-D version of the gray-level histogram kurtosis. Kurtosis measures how peaked is a distribution.
- *Diagonal Moment* measures the differences in correlation for high and low gray levels.
- *Sum Correlation* measures the asymmetry of the distribution along the diagonal of the co-occurrence matrix.

Thus, 165 features (3 different distances * 5 directions * 11 features for each case) were extracted from the co-occurrence matrix method.

It's quite interesting to see how co-occurrence matrices vary with distances and with directions for one image and to compare how they differ from one class to another. The following figures (3.2) are samples of a class 4 image: figure 3.2(a) shows matrices for $\theta = 0^o$ for the three analyzed distances; figure 3.2(b) for $\theta = 45^o$; figure 3.2(c) for $\theta = 90^o$; figure 3.2(d) for $\theta = 135^o$; figure 3.2(e) for all the unrotational one.

In a good quality muscle, tendinous structures (white stripes) must be clear and must be surrounded by black structures (muscle). This can be seen in these co-occurrence matrices: for all the analyzed directions, two small clouds of points over the diagonal can be clearly discerned. The first one, starting from the top left of the image, is associated to the black structures that surround the white stripes. The second one corresponds to the white stripes and the transition from white to black structures. It is also clear that

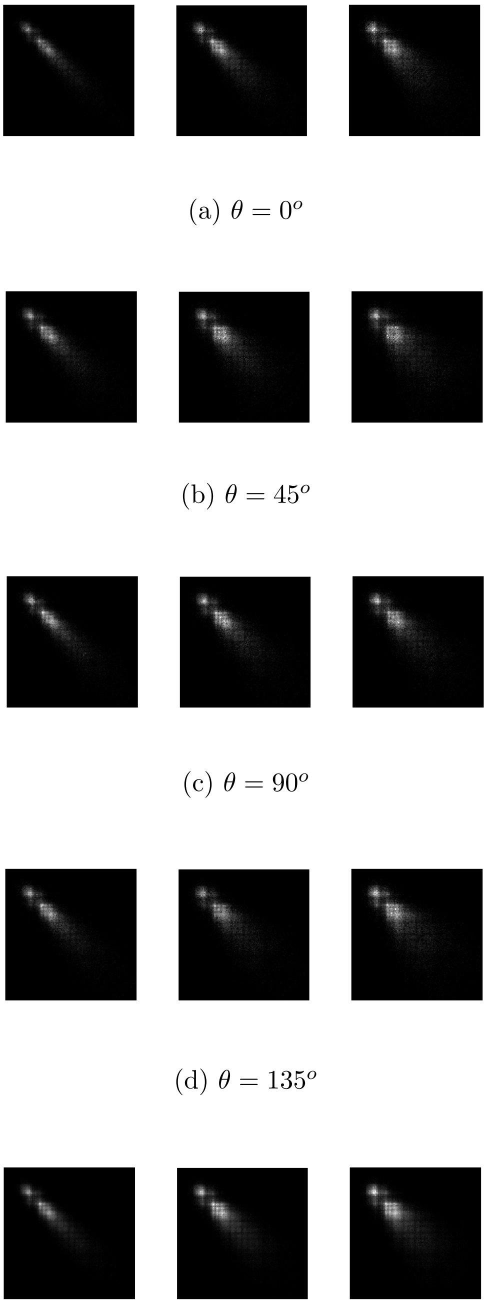

(a) $\theta = 0^o$

(b) $\theta = 45^o$

(c) $\theta = 90^o$

(d) $\theta = 135^o$

(e) Unrotational case

Figure 3.2: Co-occurrence matrices samples for quality 4

this transition is done quite fast because few intermediate gray level appear. It can be also noticed how the matrices are more dispersed when incrementing distance. This is how this matrices show that distance is getting close to elements size.

Figure 3.3 presents a similar analysis, but in this case an interclass analysis is presented. In this example just one direction is analyzed ($\theta = 45^o$), but it can be applied to all of them. In all the cases, more disperse matrices appear when incrementing distance. This effect is less clear in lower qualities. This can be explained because element sizes are smaller than in higher qualities. In quality 3 example, the transition between white black structures is slower, but higher gray levels are present. In quality 2 example, a small concentration can be seen as black structures and transition to these structures is done quite fast, but higher gray levels are quite dispersed. This could mean that original image has several echoes with medium brightness and not clear stripes. In quality 1 example, only medium gray levels are presented, so no clear structures can be seen.

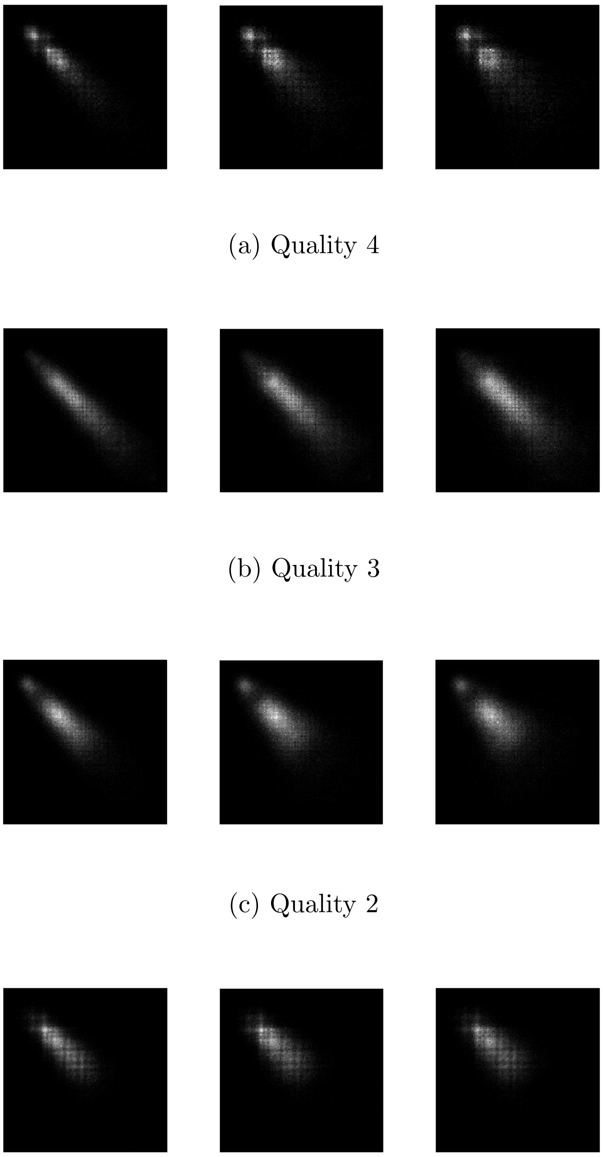

(a) Quality 4

(b) Quality 3

(c) Quality 2

(d) Quality 1

Figure 3.3: Co-occurrence matrices comparation for all qualities

Laws energy measures

The five features extracted from each resulting image were:

$$\begin{aligned}
Energy &= \sum_i \sum_j \text{TRimage}(i,j) && (3.17)\\
Mean(\mu) &= \frac{1}{MN} \sum_i \sum_j \text{TRimage}(i,j) && (3.18)\\
Variance &= \frac{1}{(M-1)N} \sum_i \sum_j (\text{TRimage}(i,j) - \mu)^2 && (3.19)\\
Skewness &= \frac{1}{MN} \sum_i \sum_j \frac{(\text{TRimage}(i,j) - \mu)^3}{Var^{\frac{3}{2}}} && (3.20)\\
Kurtosis &= \frac{1}{MN} \sum_i \sum_j \frac{(\text{TRimage}(i,j) - \mu)^4}{Var^2} && (3.21)
\end{aligned}$$

It is important to note that we have named Energy a feature that adds directly the values instead of their squares. We have done it in this way because this feature adds energy measures. Skewness and kurtosis are briefly explained in the description of diagonal moment and sum correlation features of co-occurrence matrices algorithm.

As a first approximation to the problem, we started working with the rotational invariant set of kernels to avoid managing too many features at the same time (165 co-occurrence features + 15 TR images * 5 features from each case, throws an amount of 240 features, a number comparable to the number of samples). The rotational variant case was also checked, but it gave worse results than the rotational invariant case (in this case, a total of 125 features were computed, 25 images * 5 features from each image).

Figures 3.5 to 3.19 show an example of the effect of each kernel over the quality 4 image presented in figure 3.4. No other class examples are presented because it is hardly difficult to get significant visual information, so no comparations can between classes has been done.

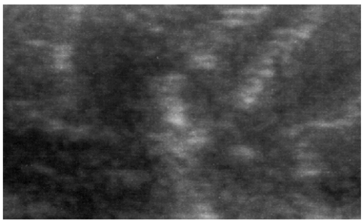

Figure 3.4: Quality 4 image base image for Laws' analysis

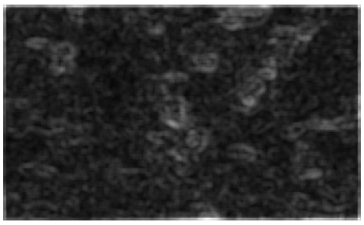

Figure 3.5: Image filtered with E5L5 mask

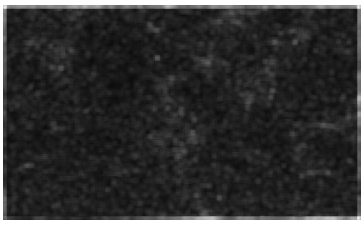

Figure 3.6: Image filtered with S5L5 mask

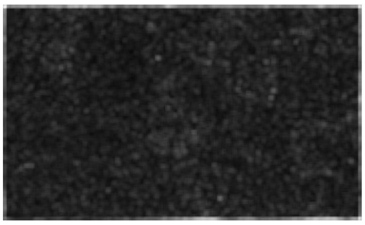

Figure 3.7: Image filtered with W5L5 mask

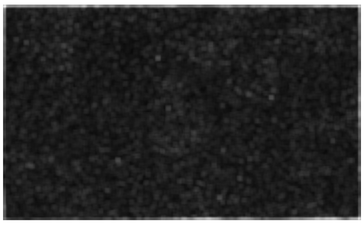

Figure 3.8: Image filtered with R5L5 mask

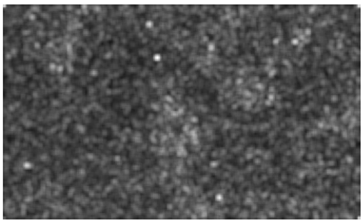

Figure 3.9: Image filtered with S5E5 mask

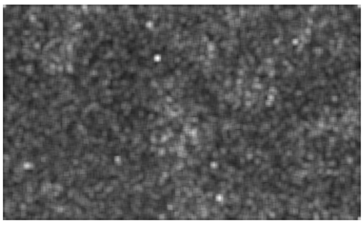

Figure 3.10: Image filtered with W5E5 mask

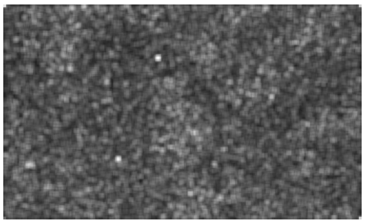

Figure 3.11: Image filtered with R5E5 mask

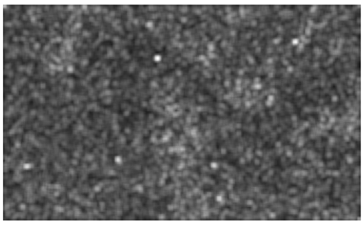

Figure 3.12: Image filtered with W5S5 mask

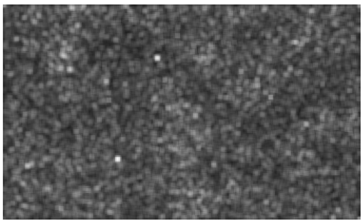

Figure 3.13: Image filtered with R5S5 mask

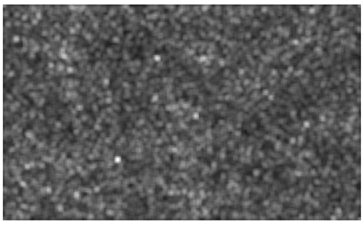

Figure 3.14: Image filtered with R5W5 mask

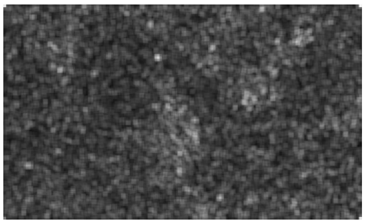

Figure 3.15: Image filtered with E5E5 mask

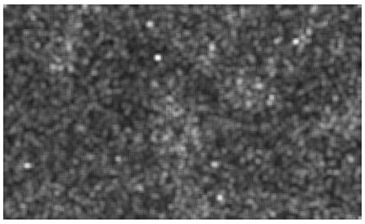

Figure 3.16: Image filtered with S5S5 mask

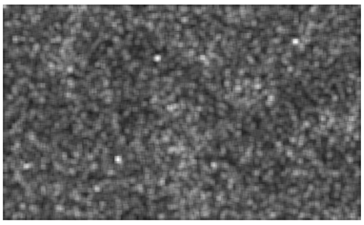

Figure 3.17: Image filtered with W5W5 mask

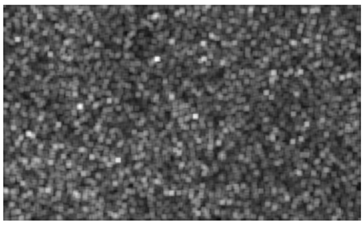

Figure 3.18: Image filtered with R5R5 mask

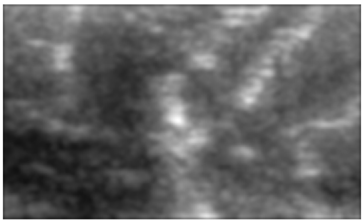

Figure 3.19: Image filtered with L5L5 mask

Chapter 4

Feature Selection and Classifier Construction

Feature selection is one of the main problems in signal processing, because extracting features (characteristics) isn't enough. This term, feature selection, refers to the selection of an optimum subset of features, and hence it is related to input dimensionality and parameter reduction problems.

Feature selection is motivated, at least, for these three main reasons:

- Many of the features are hardly correlated. Others are directly related, such as voltage and current in an electrical system.

- Some features may simply be unrelated to the problem, and hence adding noise to the system.

- Reduce computational costs, specially in real-time applications.

A good definition of feature selection is given in [20]: *Feature Selection is a process that attempts to select a subset of features, satisfying a combination of application and methodology-dependent criteria: minimizing the cardinality of the feature subset; ensuring classification accuracy does not significantly decrease; and approximating the original class distribution with the class distribution given the selected features.*

A feature selection scheme can be summarized as follows: feature subsets are somehow generated and evaluated until a stopping criterion is satisfied (figure 4.1).

There exists lots of ways of generating feature subsets. Any of them can be applied to decide candidate subsets: from exhaustive to evolutionary and

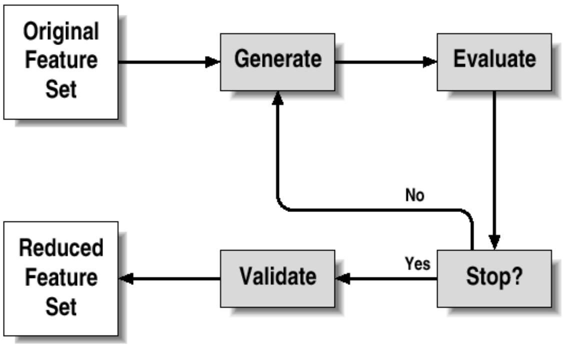

Figure 4.1: Feature selection scheme

stochastical methods.

We use a method were the training and feature selection work together to obtain the desired subset, involving sequential forward selection and a classification criteria. Due to the lack of samples in relation with the number of features, cross-validation was also applied in the training process.

4.1 Cross-validation

Cross-validation is a really well known technique used when there are not enough samples to train a system correctly, so that resampling is a must, or to check a net performance[21]. In a k-fold cross-validation, data is divided into k subsets of, approximately, equal size. The system is trained k times, each time leaving out one of the subsets from training, using this omitted subset to compute whatever error criterion. The k individual estimations are averaged, using this final result as the error estimation. Another possibility is training weights, so the averaging is applied to the resulting weights instead of the error, so the final result is an estimation of the weights.

4.2 Sequential Forward Selection

Unlike exhaustive search, sequential forward selection (SFS) is always computationally tractable. Even in the worst case, it checks a much smaller number of subsets before finishing. This technique adds predictor variables and never deletes them.

First, forward selection uses an empty set as starting subset. At the first step, FS evaluates N variable subsets, each consisting of a single variable, and selecting the one with the highest evaluation criterion. In this case, the evaluation criterion is the classification, so the variable that classifies better the images is selected. At the next step, it makes a selection among N-1 subsets, the next step from N-2 subsets, and so on. If all predictor variables are selected, at most N(N+1)/2 subsets are evaluated before the search ends. The problem with SFS is that, unlike exhaustive search, it is not guaranteed to find the subset with the highest evaluation criterion. In practice, however, many researchers have reported good results with forward selection

4.3 Classifier Construction and Results

Both training and validation steps were calculated in a MATLAB environment and further checked with the final application.

A combination of SFS with cross-validation was used in the training process. At each step of the SFS and for each analyzed case, mean square error minimization was applied to compute the system weights at each cross-validation step. Thus, let y_{obj} be a vector containing the expected values for each image of the validation set. Let y be the resulting values for each image of the validation set. Hence, the function C to minimize is:

$$C = \parallel y_{obj} - y \parallel^2 \tag{4.1}$$

Texture analysis was performed over a rectangle located between skin and bone borders. This rectangle has as top limit the lower vertical value of the skin border, and as bottom limit the higher vertical value of the bone border. Similarly, left limit has the higher horizontal value of both skin and bone border, and right limit the lower horizontal value of both borders. To avoid analyzing border points, a security margin of 5 pixels is used both in height and width.

Each class was mapped to a number: 1 for class 1, 2 for class 2, and so on. Thus, all the available data were labeled with their class. Both in training and validation steps, these labels were used as goal functions. The selected criteria to decide the image class was the distance to the labels, so the resulting value of applying the resulting weights to their related features of an image was expected to be close to its label. The selected labels were 1, 2, 3 and 4, so the threshold levels were 1.5 (limit between class 1 and 2), 2.5 (limit between class 2 and 3) and 3.5 (limit between class 3 and 4). Figure

4.2 shows validation results at each step. The best results were achieved for 28 features, with an 85.71% when success in classificating images of the validation set. It shows also that after this maximum, the system becomes over-trained and worse results are obtained.

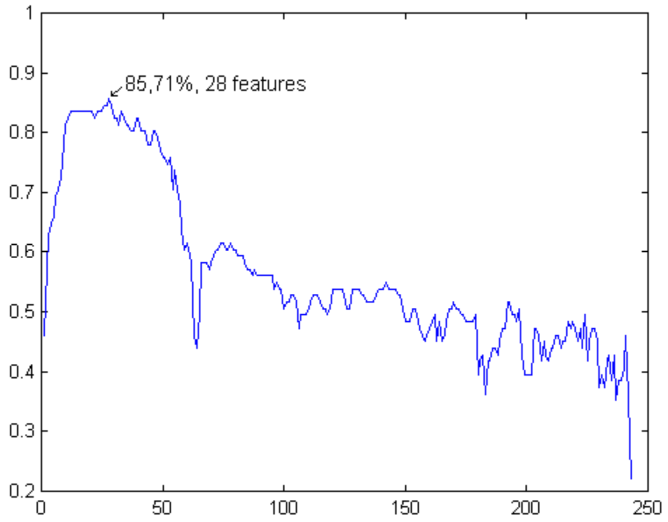

Figure 4.2: Classification results of the selected classifier. With 28 features the maximum classification rate is reached (85.71%)

Selected features were:

- Co-occurrence matrices (18):
  - $d = 3, \phi = 0$: *correlation and sum correlation*
  - $d = 5, \phi = 0$: *contrast and diagonal moment*
  - $d = 7, \phi = 0$: *energy and diagonal moment*
  - $d = 3, \phi = 45$: *energy*
  - $d = 5, \phi = 45$: *diagonal moment*
  - $d = 7, \phi = 45$: *energy, entropy, IDM and diagonal moment*
  - $d = 5, \phi = 90$: *contrast*
  - $d = 7, \phi = 90$: *IDM, correlation and diagonal moment*
  - $d = 5, \phi = 135$: *contrast*

  - $d = 7, \phi = 135$: *correlation*

- Laws' energy measures(7):
  - S5L5: *energy*
  - W5E5: *variance*
  - R5S5: *kurtosis*
  - S5S5: *variance*
  - W5W5: *variance and skewness*
  - R5R5: *skewness*

Additionally, size features were included in the analysis and also selected: area, height and width.

It must be noticed that more than half of the features from the co-occurrence matrices (10 out of 18) correspond to distance 7, so a new analysis was performed including matrices for distances 9 and 11. Results are shown in fig 4.3. An 85.71% was again the result, including just one feature for distance=11, but with 23 features instead of 28.

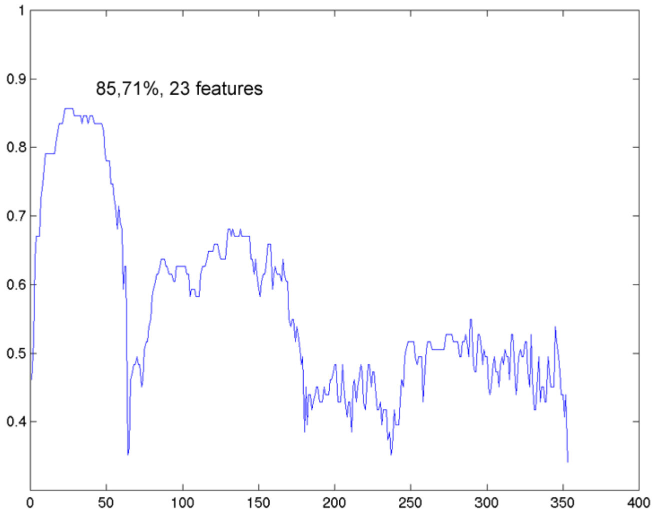

Figure 4.3: Classification results of the other classifier. With 23 features the maximum classification rate is reached (85.71%)

This reduction in the number of selected features could lead to decide to implement this new classifier instead of the selected one, but additional requirements had to be fitted, such as minimizing error impact between classes. This means that when failing in deciding an image class, this error should not be higher than one class. For example, an image of class 2 should not be classified as a class 4, but class 1 or 3 could be acceptable. Hence, an additional test was performed to check it. Results are presented in figure 4.4.

Class	1	2	3	4
1	2	5	1	0
2	0	20	1	0
3	0	3	30	1
4	0	0	2	26

(a) Results of the implemented classifier

Class	1	2	3	4
1	4	4	0	0
2	0	21	0	0
3	2	3	28	1
4	0	0	3	25

(b) Results when computing co-occurrence matrices for $d = 9, 11$

Figure 4.4: Classification results class by class for implemented classifier (figure 4.4(a)) and for classifier computing co-occurrence matrices for $d = 9, 11$, (figure 4.4(b)). Row indexes identify real classes. Column indexes identify selected classes

It can be seen that in both cases, images of class 1 are worse classified than images of the other classes. This is not surprising, because there were less images of this class than the others, as it has been explained in section 1.2 (Materials and Methods). The differences between both analyzed cases are not really significant, but one more critical error (errors of more than one class) appear when computing co-occurrence matrices for $d = 9, 11$.

As a final remark, it must be noticed that it was added in the final application the possibility of classifying an image in two classes. This possibility is activated when an image is near a threshold. In these cases, two classes appear as result: the first class (primary class) is the one normally selected; the second one (secondary class) is the class at the other side of the threshold. For example, if the resulting value of a classification is 2.6, close to 2.5 threshold, the primary class is 3 and the secondary class is 2.

Chapter 5

Conclusions

5.1 Achievements

In this work we have presented the implementation of a classifier for US images of the masseteric muscle. This classifier has been implemented following this steps:

1. locate the muscle via detecting its borders
2. application of a texture analysis over a selected region of the muscle
3. combine linearly the extracted features and mapping the result to a class (or classes)
4. developement of an interface for automatic classification

Feature selection was developed by combining sequential forward selection with cross-validation, in order to find which features contained classification information and to decide their importance, by computing their associated weights.

Dual class results are presented when system computes ambiguous results. This additional functionality permits receiving more accurate information in classification terms. Finally, it was also achieved to compute few critical results.

5.2 Future Work

Due to the nature of the application, it can be easily adapted to other US muscle images. It just needs a set of previously classified images. In this point, it must be noticed that in training step, muscle selected area was decided by a non-expert user, so this must be taken into account for any future developement, because it can be useful to get a better trained system and, hence, to get a better classifier.

Another possible improvement could be developing full automatic classifier, automatically detecting muscle borders.

It is also possible to insert the application in the US machine. If this improvement were combined with the automatical border detection, it could be possible to have an US machine with a healthy integrated classifier. This improvement is closely related with another problem that could not be solved because of the nature of the provided images. In an integrated application, there is no need of printing the image and then scan it. These steps also adds noise to the original sample and better results could be reached if they were eliminated.

Appendix A

User Manual

When executing the program, a browser appears to select the desired image. It must be a scanned image, at 300x300dpi of resolution and then it must be saved in .bmp format, with 24 bits per pixel. Any comercial scanner can fit these requirements.

Once the image has been selected, a window appears containing the central part of the selected image. Figure A.1 is shown as example.

Menu options

There are two options in the menu bar: Muscle capture and Image Mode (figure A.2).

- *Muscle capture* offers the possibility of selecting the image area where the analysis will be performed by selecting the borders (Borders option) or directly by selecting four points to directly configure the rectangle (Rectangle option).

- *Image mode* offers the possibility to analyze images directly extracted from an US machine or scanned images previously printed. This menu is disabled. It has been included for further improvements.

Menu options must be selected before usign any other part of the application.

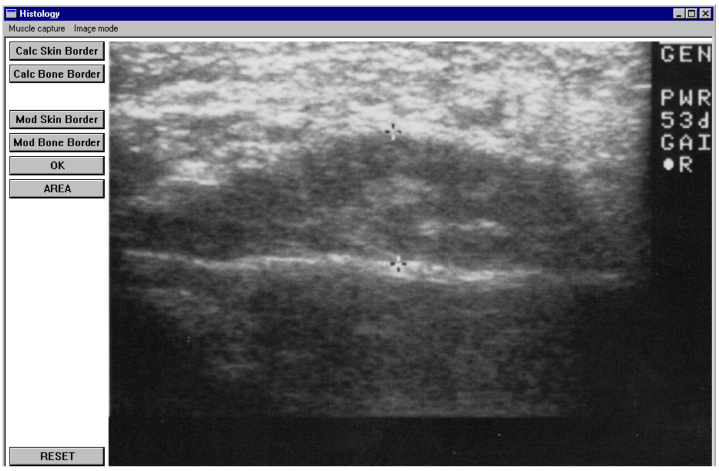

Figure A.1: View of the application window

Buttons

There are seven buttons in the window: Calc Skin Border, Calc Bone Border, Mod Skin Border, Mod Bone Border, OK, AREA and RESET.

- *Calc Skin Border* Calculates the skin border once both initial and ending point have been set.
- *Calc Bone Border* Calculates the bone border once both initial and ending point have been set.
- *Mod Skin Border* When clicking on this option, all the points set by the user will be used to find the skin border.
- *Mod Bone Border* When clicking on this option, all the points set by the user will be used to find the bone border.
- *OK* Once both borders have been calculated or the area has been directly selected, clicking this button computes image class.
- *AREA* This button is used to directly set the area to be analyzed.

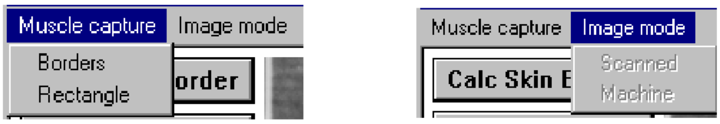

Figure A.2: Menu contents of the application

- *RESET* By clicking this button a browser is opened to select a new image (or the same) to analyze.

It must be noticed that options selected in the menu affect those buttons. If Rectangle option has been selected, Calc Skin Border, Calc Bone border, Mod Skin Border and Mod Bone border buttons do not work. If Borders options is selected, AREA button do not work.

General Procedure

There are two possible procedures depending on which Muscle capture option is selected:

1. Computing borders: there is no problem with starting calculating skin or bone border. To compute the skin border, first click on Mod Skin Border button. Then starting and ending points must be set. At this point, skin border can be calculated by clicking on Calc Skin Border button. If the resulting border does not fit to the real one, additional points can be set to help the program to get it. These point shoul be

set in areas to which program cannot compute, such as whithe thick stripes close to the border. These points can be set before calculating any border. Points are set by left clicking on the image. Right clicking will remove the closest user-set point. The same process must be done to compute tha bone border but using Mod Bone Border and Calc Bone Border buttons. Once both borders have been selected clicking on OK button will perform the classification of the muscle.

2. Area selection: select four points to define the rectangular area to be analyzed. The highest restricting conditions will be applied (minimum upper value, maximum lower value, etc.). Once these points are set, clicking on OK button will perform the classification of the muscle.

For any doubts, please contact: rbartolome@ambtu.bcn.es

Bibliography

[1] N.-D. Kim, V. Amin, D. Wilson, G. Rouge, and S. Udpa, "Multiresolutional texture analysis for ultrasound tissue characterization," *Nondestructive Testing and Evaluation, special issue on Biomedical applications*, no. 4, pp. 201–215, 1998.

[2] N.-D. Kim, L. Booth, V. Amin, J. Lim, and S. Udpa, "Ultrasonic image processing for tendon injury evaluation," *Proceedings of the IEEE-SP International Symposium on Time-Frequency and Time-Scale analysis*, USA, 1998.

[3] M. Masseroli, M. Cothren, D. Meier, and et al., "Quantification of intramural calcification in coronary intravascular ultrasound images with automated image analysis," *Am Heart J*, vol. 136, no. 1, pp. 78–86, 1998.

[4] T. Gustavsson, Q. Liang, I. Wendelhag, and J. Wikstrand, "A dynamic programming procedure for automated ultrasonic measurement of the carotid artery," *Proceedings IEEE Computers Cardiology*, pp. 297–300, 1994.

[5] R. J. Kozick, "Detecting interfaces on ultrasound images of the carotid artery by dynamic programming," *SPIE*, pp. 233–241, 1996.

[6] Q. Liang, I. Wendelhag, J. Wikstrand, and T. Gustavsson, "A multiscale dynamic programming procedure for boundary detection in ultrasonic artery images," *IEEE Transactions on Medical Imaging*, no. 2, pp. 127–142, 2000.

[7] J. Slansky, "Image segmentation and feature selection," *IEEE Transactions on Systems, Man and Cybernetics*, no. 4, pp. 237–247, 1978.

[8] B. Jahne, "Digital image processing."

[9] Wilson and Spaan, "Image segmentation and uncertainty."

[10] A. K. Jain, "Fundamentals of image processing."

[11] R. C. Gonzalez and R. E. Woods, “Digital image processing.”

[12] I. S. 610.4-1990, “Ieee standard glossary of image processing and pattern recognition terminology,” *IEEE Press*, New York, 1990.

[13] R. M. Haralick, “Statistical and structural approaches to texture,” *Proceedings IEEE*, vol. 67, no. 5, pp. 786–804, 1979.

[14] U. Raeth, D. Schlaps, B. Limberg, I. Zuna, A. Lorenz, G. van Kaick, W. J. Lorenz, and B. Kommerell, “Diagnostic accuracy of computerized b-scan texture analysis and conventional ultrasonography in diffuse parenchymal and malignant liver disease,” *J. Clin. Ultrasound*, pp. 87–99, 1985.

[15] F. M. J. Valckx and J. M. Thijssen, “Texture classification of echographic images by means of the co-occurrence matrix,” *Acoust. Imag.*, pp. 299–302, 1996.

[16] C.-M. Wu, Y.-C. Chen, and K.-S. Hsieh, “Texture features for classification of ultrasonic liver images,” *IEEE Transactions on Medical Imaging*, pp. 141–152, Apr. 1992.

[17] A. P. Pentland, “Fractal-based description of natural scenes,” *IEEE Transactions on Pattern Analysis and Machine Intelligence*, no. 6, pp. 661–674, 1984.

[18] R. M. Haralick, K. Shanmugam, and I. Distein, “Textural features for image classification,” *IEEE Transactions on Systems, Man and Cybernetics*, no. SMC-3, pp. 610–621, 1973.

[19] K. Laws, “Textured image segmentation,” *Ph.D. Dissertation, University of Southern California*, January, 1980.

[20] M. Dash and H. Liu, “Feature selection for classification,” *Intelligent Data Analysis - An International Journal*, no. 3, pp. 374–385, 1997.

[21] G. Torheim, F. Godtliebsen, D. Axelson, K. A. Kvistad, A. Haraldseth, and P. A. Rinck, “Feature extraction and classification of dynamic contrast-enhanced t2*-weighted breast image data,” *IEEE Transactions on Medical Imaging*, no. 12, pp. 1293 – 1301, 2001.